

Hyperon properties in finite nuclei using realistic YN interactions

I. Vidaña, A. Polls, A. Ramos

Departament d'Estructura i Constituents de la Matèria, Universitat de Barcelona, E-08028

Barcelona, Spain

M. Hjorth-Jensen

Nordita, Blegdamsvej 17, DK-2100 København Ø, Denmark

Abstract

Single-particle energies of Λ and Σ hyperons in several nuclei are obtained from the relevant self-energies. The latter are constructed within the framework of a perturbative many-body approach employing present realistic hyperon-nucleon interactions such as the models of the Jülich and Nijmegen groups. The effects of the non-locality and energy-dependence of the self-energy on the bound states are investigated. It is also shown that, although the single-particle hyperon energies are well reproduced by local Woods-Saxon hyperon-nucleus potentials, the wave functions from the non-local self-energy are far more extended. Implications of this behavior on the mesonic weak decay of Λ hypernuclei are discussed.

PACS Numbers: 21.80.+a, 13.75.Ev, 21.65.+f.

Keywords: Hypernuclei, YN interaction, G -matrix, self-energy.

Typeset using REVTeX

I. INTRODUCTION

Hypernuclei are bound systems of neutrons, protons and one or more strange baryons, such as the Λ or Σ hyperons. Understanding the behavior of hypernuclei (how they are produced, their spectroscopy and decay mechanisms) has been the subject of intense investigations during the last decades, see e.g., Refs. [1–10].

One of the main goals of such studies is to explore how the presence of the new degree of freedom (strangeness) alters and broadens the knowledge achieved from conventional nuclear physics. Several features of the Λ single-particle properties in the nucleus, being essentially different from those of the nucleon, have clearly emerged from these efforts. It is well accepted nowadays that the depth of the Λ -nucleus potential is around -30 MeV, which is 20 MeV less attractive than the corresponding nucleon-nucleus one. The spin-orbit splittings of single particle levels in Λ hypernuclei were found to be much smaller than their nucleonic counterparts [11], typically more than one order of magnitude. Moreover, the Λ , contrary to the nucleon, maintains its single-particle character even for states well below the Fermi surface [12,13] indicating a weaker interaction with other nucleons. Studies of the mesonic weak decay of light Λ hypernuclei [14–16] have shown that the data [17] clearly favour Λ -nucleus potentials which show a repulsion at short distances. This seems also to be a characteristic of the Σ -nucleus potential for light Σ -hypernuclei [18], which reproduces the recently measured bound Σ^+ state in ${}^4_2\text{He}$ with the in-flight ${}^4\text{He}(K^-, \pi^-)$ reaction [19]. This experiment confirms, with new and better statistics, the earlier results from the ${}^4\text{He}(\text{stopped } K^-, \pi^-)$ reaction [20].

Attempts to derive the hyperon properties in a nucleus have followed several approaches. A Λ -nucleus potential of Woods-Saxon type reproduces reasonably well the measured Λ single-particle energies of medium to heavy hypernuclei [21–23]. Non localities and density dependent effects, included in non-relativistic Hartree-Fock calculations using Skyrme hyperon-nucleon (YN) interactions [24–27], improve the overall fit to the single-particle binding energies. The properties of hypernuclei have also been studied in a relativistic

framework, such as Dirac phenomenology [28,29] or relativistic mean field theory [30–37].

Microscopic calculations, which aim at relating the hypernuclear observables to the bare YN interaction, are also available. This approach is especially interesting because it can be used to put further constraints on the YN interactions, which are not completely determined by the limited amount of scattering data due, essentially, to the experimental difficulties associated with the short lifetime of hyperons and low intensity beam fluxes. Microscopic hypernuclear structure calculations are performed with an effective YN interaction (G -matrix) obtained from the bare YN potential through a Bethe-Goldstone equation. The comparison with data may therefore further help in constraining the YN potentials. In several microscopic calculations a Gaussian parametrizations of the G -matrix calculated in nuclear matter at an average density [37–40] was employed. Furthermore, a G -matrix obtained directly in finite nuclei was used to study the single-particle energy levels of various hypernuclei [41] or as an effective interaction in a calculation of the ${}_{\Lambda}^{17}\text{O}$ spectrum [42].

Along similar lines, the authors of Ref. [43] derived microscopically the Λ self-energy in ${}_{\Lambda}^{17}\text{O}$, starting from realistic hyperon-nucleon interactions. The starting point in the latter calculations is a nuclear matter G -matrix at a fixed energy and density, which is used to calculate the self-energy for the finite nucleus including corrections up to second order. The obtained self-energy for the Λ is non-local and depends on the energy of the hyperon. Solving the Schrödinger equation with this self-energy it is possible to determine the single-particle energies and wave functions of the bound hyperon. The approach also provides automatically the real and imaginary part of the hyperon optical potential at positive energies and, therefore, allows to study the hyperon-nucleus scattering properties. The method was first employed to study the nucleon and Δ properties in nuclei [44,45] and later applied to calculate the s -wave non-local Λ self-energy in ${}_{\Lambda}^{17}\text{O}$, from which the single-particle Λ binding energy was obtained [43].

The aim of the present work is to extend the calculations of Ref. [43] in order to derive s and p -wave Λ single-particle energies for a variety of Λ hypernuclei, from ${}_{\Lambda}^{17}\text{O}$ to ${}_{\Lambda}^{209}\text{Pb}$. The Σ single-particle energies obtained for different potentials are also discussed. The YN

potentials employed are the Nijmegen soft-core [46] and the Jülich [47] interactions. Eventual differences in single-particle binding energies may therefore help in further constraining the YN interactions.

In Sect. II, we present the formalism which consists of obtaining, first, the nuclear matter G -matrix at fixed density and starting energy parameter in the center of mass frame and, next, performing a second order calculation to derive the finite nucleus G -matrix from which one can obtain the hyperon self-energy for the different single-particle orbits. This self-energy can in turn be used to define a single-particle potential in a Schrödinger equation in order to obtain the corresponding single-particle binding energies. Nuclear matter results and a discussion on the convergence of our method is presented in Sect. III A. An important point raised in the latter section is that the single-particle hyperon energies calculated at first order with a nuclear matter G -matrix depend quite strongly on the fixed starting energy and density employed. The Λ single-particle energies for a variety of hypernuclei are shown in Sect. III B, where local equivalent Woods-Saxon potentials to represent our non-local self-energy are also derived. Finally, our conclusions are presented in Sect. IV.

II. FORMALISM

In this section we present the formalism to obtain the hyperon single-particle energies in finite hypernuclei using an effective interaction derived microscopically from realistic YN interactions, for which we take the Nijmegen soft core [46] and Jülich [47] potentials. Although the formalism was already described in Ref. [43], part of it will be repeated here in order to set up the notation used later in the description of the results. In the first place, we solve the G -matrix in nuclear matter at a fixed density, center of mass momentum and energy. Next, we transform this G -matrix into an effective interaction for the finite hypernucleus from which we can obtain the hyperon self-energy. Finally, we use this self-energy in a Schrödinger equation to derive the single-particle energies and the corresponding wave functions of the bound states.

A. Nuclear matter YN G -matrix

The nuclear matter YN G -matrix is solved in momentum space and the two-particle YN states are defined in terms of relative and the center-of-mass momenta, \mathbf{k} and \mathbf{K} , given by

$$\mathbf{k} = \frac{M_N \mathbf{k}_Y - M_Y \mathbf{k}_N}{M_N + M_Y},$$

$$\mathbf{K} = \mathbf{k}_N + \mathbf{k}_Y ,$$

where \mathbf{k}_N and \mathbf{k}_Y are the nucleon and hyperon momenta, respectively. Using an angle-averaged Pauli operator, we perform a partial wave decomposition of the Bethe-Goldstone equation, which, in terms of the quantum numbers of the relative and center-of-mass motion (RCM), is written as

$$\begin{aligned} \langle (Y''N)k''l''KL(\mathcal{J})S''T_z | G(\omega_{NM}) | (YN)klKL(\mathcal{J})ST_z \rangle = \\ \langle (Y''N)k''l''KL(\mathcal{J})S''T_z | V | (YN)klKL(\mathcal{J})ST_z \rangle \\ + \sum_{l'} \sum_{S'} \sum_{Y'=\Lambda\Sigma} \int k'^2 dk' \langle (Y''N)k''l''KL(\mathcal{J})S''T_z | V | (Y'N)k'l'KL(\mathcal{J})S'T_z \rangle \\ \times \frac{Q(k', K)}{\omega_{NM} - \frac{K^2}{2(M_N+M_{Y'})} - \frac{k'^2(M_N+M_{Y'})}{2M_N M_{Y'}} - M_{Y'} + M_Y} \\ \times \langle (Y'N)k'l'KL(\mathcal{J})S'T_z | G(\omega_{NM}) | (YN)klKL(\mathcal{J})ST_z \rangle , \end{aligned} \quad (1)$$

where Q is the nuclear matter Pauli operator, V is the YN potential and ω_{NM} is the nuclear matter starting energy which corresponds to the sum of non-relativistic single-particle energies of the interacting nucleon and hyperon. Note that kinetic energies are used in the intermediate $Y'N$ states and $M_Y - M_{Y'}$ accounts for the mass difference of the initial and intermediate hyperon. The variables k , k' , k'' and l , l' , l'' denote relative momenta and angular momenta, respectively, while K and L are the quantum numbers of the center-of-mass motion. The total angular momentum, spin and isospin projection of the YN pair are denoted by \mathcal{J} , S and T_z , respectively.

B. The hyperon single-particle potential U_Y in nuclear matter

In the Brueckner-Hartree-Fock approach the hyperon single-particle potential U_Y is obtained self-consistently by the following sum of diagonal G -matrix elements:

$$U_Y(k_Y) = \int_{k_N \leq k_F} d^3 k_N \langle Y\mathbf{k}_Y, N\mathbf{k}_N | G(\varepsilon_N(k_N) + \varepsilon_Y(k_Y)) | Y\mathbf{k}_Y, N\mathbf{k}_N \rangle , \quad (2)$$

where $\varepsilon_{N(Y)}(k_{N(Y)}) = k_{N(Y)}^2/(2M_{N(Y)}) + U_{N(Y)}(k_{N(Y)})$ is the single-particle energy of the nucleon (hyperon). Using the partial wave decomposition of the G -matrix, the single-particle potential U_Y can be rewritten as

$$U_Y(k_Y) = \frac{(1 + \xi_Y)^3}{2(2t_Y + 1)} \sum_{\mathcal{J}, l, S, T} (2\mathcal{J} + 1)(2T + 1) \times \int_0^{k_{max}} k^2 dk f(k, k_Y) \langle YN; klST_z | G^{\mathcal{J}}(\varepsilon_N(k_N) + \varepsilon_Y(k_Y)) | YN; klST_z \rangle , \quad (3)$$

where an average over the hyperon spin and isospin (t_Y) has been performed and the weak center-of-mass dependence of the G -matrix has been neglected. In Eq. (3), k is the relative momentum of the YN pair, $\xi_Y = M_N/M_Y$, k_{max} is given by

$$k_{max} = \frac{k_F + \xi_Y k_Y}{1 + \xi_Y} \quad (4)$$

and the weight function $f(k, k_Y)$ by

$$f(k, k_Y) = \begin{cases} 1 & \text{for } k \leq \frac{k_F - \xi_Y k_Y}{1 + \xi_Y} , \\ 0 & \text{for } |\xi_Y k_Y - (1 + \xi_Y)k| > k_F , \\ \frac{k_F^2 - [\xi_Y k_Y - (1 + \xi_Y)k]^2}{4\xi_Y(1 + \xi_Y)k_Y k} & \text{otherwise} \end{cases} \quad (5)$$

In the discussion, we will associate the binding energy of the hyperon to its single-particle energy:

$$B_Y(k_Y) \equiv \varepsilon(k_Y) = \frac{k_Y^2}{2M_Y} + U_Y(k_Y) \quad (6)$$

C. Evaluation of the hyperon self-energy

The self-energy of the Λ or Σ hyperon in a finite hypernucleus can be obtained, in the Hartree-Fock scheme, using a finite nucleus G -matrix as an effective YN interaction. However, our G -matrix has been obtained in nuclear matter and, in particular, the intermediate propagator (that involves the Pauli operator and energy denominator) is very different than the corresponding one in a finite hypernucleus. One can, nevertheless, find the appropriate finite nucleus G -matrix, G_{FN} , by relating it to the nuclear matter G -matrix through the following integral equation written in schematic form:

$$\begin{aligned} G_{FN} &= G + G \left[\left(\frac{Q}{e} \right)_{FN} - \left(\frac{Q}{e} \right)_{NM} \right] G_{FN} \\ &= G + G \left[\left(\frac{Q}{e} \right)_{FN} - \left(\frac{Q}{e} \right)_{NM} \right] G \\ &\quad + G \left[\left(\frac{Q}{e} \right)_{FN} - \left(\frac{Q}{e} \right)_{NM} \right] G \left[\left(\frac{Q}{e} \right)_{FN} - \left(\frac{Q}{e} \right)_{NM} \right] G + \dots , \end{aligned} \quad (7)$$

which involves the nuclear matter G -matrix (labelled G throughout the text) and the difference between the finite nucleus and nuclear matter propagators. The latter account for the relevant intermediate states. In the practical calculations we will approximate the expansion up to the second order in the nuclear matter G -matrix

$$G_{FN} \simeq G + G \left[\left(\frac{Q}{e} \right)_{FN} - \left(\frac{Q}{e} \right)_{NM} \right] G . \quad (8)$$

Therefore, in the evaluation of the hyperon self-energy we take into account the diagrams displayed in Fig. 1, where the wiggly interaction lines represent the nuclear matter G -matrix. Diagram 1(a) represents the first term on the right hand side of Eq. (8) which, by analogy to the nuclear case, will be referred to as the Hartree-Fock contribution. Diagram 1(b) stands for the second order correction, where the intermediate propagator has to be viewed as the difference of propagators appearing in Eq. (8).

We will consider the incoming (outcoming) hyperon as a plane wave and the nucleon hole states as harmonic oscillator ones, so the two-body wave function will be a mixed representation of both single-particle states given by

$$|(n_h l_h j_h t_{z_h})(k_Y l_Y j_Y t_{z_Y})JT_z\rangle = \int k_h^2 dk_h R_{n_h l_h}(\alpha k_h) |(k_h l_h j_h t_{z_h})(k_Y l_Y j_Y t_{z_Y})JT_z\rangle, \quad (9)$$

where $n_h l_h j_h t_{z_h}$ and $k_Y l_Y j_Y t_{z_Y}$ are the quantum numbers of the nucleon hole state and the hyperon state, respectively. Further, α is the oscillator parameter appropriate to describe the single-particle wave functions of the bound nucleons in the nuclear core. It is defined as

$$\alpha = \frac{\hbar c}{\sqrt{M_N \hbar \omega}} \quad (10)$$

with $\hbar \omega$ chosen as the following function of the mass number

$$\hbar \omega = 45A^{-\frac{1}{3}} - 25A^{-\frac{2}{3}}. \quad (11)$$

Typical matrix elements needed in the calculation are

$$\langle (k_Y l_Y j_Y t_{z_Y})(n_h l_h j_h t_{z_h})JT_z | G | (k'_Y l_Y j_Y t_{z_Y})(n_h l_h j_h t_{z_h})JT_z \rangle, \quad (12)$$

for the Hartree-Fock diagram of Fig. 1(a), or

$$\langle (k_Y l_Y j_Y t_{z_Y})(n_h l_h j_h t_{z_h})JT_z | G | (YN)klKL(\mathcal{J})ST_z \rangle, \quad (13)$$

appearing in the second-order diagram of Fig. 1(b).

Using Eq. (9), the mixed representation states appearing in Eqs. (12) and (13) can be expressed in terms of momentum and angular momentum variables in the laboratory frame. Then, with appropriate transformation coefficients [48,49], one can express the two-body states with laboratory coordinates in terms of the variables in the RCM system used in the solution of the G -matrix¹

¹Note the distinction between k_a and k and l_a and l . With the notation k_a or l_a we will refer to the quantum numbers of the single-particle state, whereas l or k without subscripts refer to the coordinates of the relative motion.

$$\begin{aligned}
|(k_a l_a j_a t_{z_a})(k_b l_b j_b t_{z_b})JT_z\rangle &= \sum_{lL\lambda S\mathcal{J}} \int k^2 dk \int K^2 dK \begin{Bmatrix} l_a & l_b & \lambda \\ \frac{1}{2} & \frac{1}{2} & S \\ j_a & j_b & J \end{Bmatrix} \\
&\times (-1)^{\lambda+\mathcal{J}-L-S} \hat{\mathcal{J}} \hat{\lambda}^2 \hat{j}_a \hat{j}_b \hat{S} \begin{Bmatrix} L & l & \lambda \\ S & J & \mathcal{J} \end{Bmatrix} \\
&\times \langle klKL|k_a l_a k_b l_b\rangle |klKL(\mathcal{J})SJT_z\rangle,
\end{aligned} \tag{14}$$

where $\hat{x} = \sqrt{2x+1}$ and $\langle klKL|k_a l_a k_b l_b\rangle$ are the transformation coefficients from the RCM system to the laboratory system.

We can construct now the expressions for the various diagrams considered in this work. The first order term of Fig. 1(a) yields a real and energy-independent contribution to the self-energy given by

$$\begin{aligned}
\mathcal{V}_{HF}(k_Y k'_Y l_Y j_Y t_{z_Y}) &= \frac{1}{\hat{j}_Y^2} \sum_{\mathcal{J}} \sum_{n_h l_h j_h t_{z_h}} \hat{j}^2 \\
&\times \langle (k_Y l_Y j_Y t_{z_Y})(n_h l_h j_h t_{z_h})JT_z | G | (k_Y l_Y j_Y t_{z_Y})(n_h l_h j_h t_{z_h})JT_z \rangle,
\end{aligned} \tag{15}$$

where $k_Y (k'_Y) l_Y j_Y t_{z_Y}$ are the quantum numbers of the incoming(outcoming) hyperon.

The computation of the contribution coming from the two-particle-one-hole ($2p1h$) diagram of Fig. 1(b) requires a little more work. First, we evaluate the imaginary part of the second term in Eq. (8). This term has an explicit energy dependence. It reads

$$\begin{aligned}
\mathcal{W}_{2p1h}^{(1)}(k_Y k'_Y l_Y j_Y t_{z_Y}, \omega) &= -\frac{1}{\hat{j}_Y^2} \sum_{n_h l_h j_h t_{z_h}} \sum_{\mathcal{J}} \sum_{lL S \mathcal{J}} \sum_{Y'=\Lambda\Sigma} \int k^2 dk \int K^2 dK \hat{J} \hat{T} \\
&\times \langle (k'_Y l_Y j_Y t_{z_Y})(n_h l_h j_h t_{z_h})JT_z | G | (Y'N)klKL(\mathcal{J})SJT_z \rangle \\
&\times \langle (Y'N)klKL(\mathcal{J})SJT_z | G | (k_Y l_Y j_Y t_{z_Y})(n_h l_h j_h t_{z_h})JT_z \rangle \\
&\times \pi \delta \left(\omega + \varepsilon_h - \frac{K^2}{2(M_N + M_{Y'})} - \frac{k^2(M_N + M_{Y'})}{2M_N M_{Y'}} - M_{Y'} + M_Y \right),
\end{aligned} \tag{16}$$

where ω is the energy of the hyperon measured with respect to the hyperon rest mass. The

single-hole energies ε_h have been taken equal to the experimental single-particle energies in most of the nuclei studied (e.g., ^{12}C , ^{16}O , ^{40}Ca) and have been calculated from a Woods-Saxon potential with Spin-Orbit and Coulomb terms appropriately fitted in other cases (e.g., ^{90}Zr and ^{208}Pb). The quantities $klKL(\mathcal{J})SJT_z$ are the quantum numbers of the intermediate $Y'N$ states. Next, we obtain the real part through a dispersion relation

$$\mathcal{V}_{2p1h}^{(1)}(k_Y k'_Y l_Y j_Y t_{z_Y} \omega) = \frac{P}{\pi} \int_{-\infty}^{\infty} \frac{\mathcal{W}_{2p1h}(k_Y k'_Y l_Y j_Y t_{z_Y} \omega')}{\omega' - \omega} d\omega', \quad (17)$$

where P means a principal value integral.

Finally, we must subtract the $2p1h$ correction term coming from the nuclear matter intermediate propagator (third term in Eq. (8)). It reads

$$\begin{aligned} \mathcal{V}_{2p1h}^{(2)}(k_Y k'_Y l_Y j_Y t_{z_Y}) &= \frac{1}{\hat{j}_Y^2} \sum_{n_h l_h j_h t_{z_h}} \sum_J \sum_{lLS\mathcal{J}} \sum_{Y'=\Lambda\Sigma} \int k^2 dk \int K^2 dK \hat{J}\hat{T} \\ &\times \langle (k'_Y l_Y j_Y t_{z_Y})(n_h l_h j_h t_{z_h})JT_z | G | (Y'N)klKL(\mathcal{J})SJT_z \rangle \\ &\times \langle (Y'N)klKL(\mathcal{J})SJT_z | G | (k_Y l_Y j_Y t_{z_Y})(n_h l_h j_h t_{z_h})JT_z \rangle \\ &\times Q(k, K) \left(\omega_{NM} - \frac{K^2}{2(M_N + M_{Y'})} - \frac{k^2(M_N + M_{Y'})}{2M_N M_{Y'}} - M_{Y'} + M_Y \right)^{-1}, \end{aligned} \quad (18)$$

where Q is the nuclear matter Pauli operator and ω_{NM} is the nuclear matter starting energy. This term only contributes to the real part of the hyperon self-energy and avoids the double counting over intermediate $Y'N$ states contained already in the nuclear matter G -matrix of the Hartree-Fock contribution \mathcal{V}_{HF} .

In summary, the self-energy of the hyperon reads

$$\Sigma(k_Y k'_Y l_Y j_Y \omega) = V(k_Y k'_Y l_Y j_Y \omega) + iW(k_Y k'_Y l_Y j_Y \omega), \quad (19)$$

with the real part given by

$$V(k_Y k'_Y l_Y j_Y \omega) = \mathcal{V}_{HF}(k_Y k'_Y l_Y j_Y) + \mathcal{V}_{2p1h}^{(1)}(k_Y k'_Y l_Y j_Y \omega) - \mathcal{V}_{2p1h}^{(2)}(k_Y k'_Y l_Y j_Y) \quad (20)$$

and the imaginary part by

$$W(k_Y k'_Y l_Y j_Y \omega) = \mathcal{W}_{2p1h}^{(1)}(k_Y k'_Y l_Y j_Y \omega). \quad (21)$$

The self-energy can then be inserted as a single-particle potential in a Schrödinger equation in order to investigate bound and scattering states of a hyperon in a finite nucleus. The different approximations to the self-energy, i.e., whether we include the $2p1h$ contribution or not, result in different single-particle hamiltonians. We solve the Schrödinger equation by diagonalizing the corresponding single-particle hamiltonian in a complete basis within a spherical box of radius R_{box} following the procedure outlined in [43]. This method is especially suitable for non-local potentials defined either in coordinate or in momentum space [44,45].

III. RESULTS AND DISCUSSION

In this section we present and discuss results for Λ and Σ hypernuclei using two realistic interactions: Nijmegen soft core [46] and Jülich B [47].

A. Dependence of results on the starting energy

As described before, our method provides the binding energies of the different hyperon orbits in finite hypernuclei starting from a G -matrix calculated in nuclear matter in the YN center-of-mass frame at fixed starting energy ω_{NM} and Fermi momentum k_F . By adding the $2p1h$ correction to the Hartree-Fock term one incorporates, up to second order in the nuclear matter G -matrix, the correct energy dependence and Pauli blocking factor in the finite nucleus. Therefore, the complete calculation ($HF + 2p1h$) has to be viewed as a Hartree-Fock approach which uses an effective interaction derived microscopically with the appropriate density and energy dependence of the hypernucleus under study. This is in contrast to previous calculations [37–40] where the determination of the finite hypernucleus effective interaction from the nuclear matter G -matrix implied a sort of average over the nuclear density. In these works several local and energy independent effective YN interactions of Gaussian form (YNG) were derived by parametrizing the corresponding nuclear matter G -matrices obtained from various YN potentials. The parametrization of the G -matrix into

a local effective interaction YNG to be used in finite hypernuclei calculations required the use of an appropriate value of the Fermi momentum k_F . This value was determined, for each nucleus, by averaging the corresponding nuclear density weighted by the modulus squared of the Λ single-particle wave function of the single-particle level under study. The parameters of the effective YNG interaction were adjusted to reproduce the Λ potential energy $U_\Lambda(0)$ in nuclear matter at the average value of k_F . With these parametrizations, Λ single-particle energies and excited hypernuclear levels in several Λ hypernuclei were obtained through a shell-model calculation, with the aim of learning about the bare YN interaction.

It therefore seems appropriate to explore, using our method, how much the hyperon single-particle energy depends on the starting energy (and density) of the nuclear matter G -matrix used in the calculation. This will allow us to assess how reliable energy independent effective interactions obtained from local density averages might be.

Let us first show, in Fig. 2, the binding energy $B_Y(k=0)$ of a Λ (curves on the left) or a Σ (curves on the right) in nuclear matter at $k_F = 1.36 \text{ fm}^{-1}$ as a function of the starting energy parameter $\omega = \omega_{NM} + \Delta = \langle B_N \rangle + B_Y(k=0) + \Delta$, where $\langle B_N \rangle = -50 \text{ MeV}$ is an average of the nucleon binding energy over the Fermi sea and $\Delta = M_Y - M_\Lambda$. The long-dashed (full) lines are for the Nijmegen soft core (Jülich B) interaction. An estimate of the self-consistent solution is obtained where the line $\omega = \omega_{NM} + \Delta = \langle B_N \rangle + B_Y(k=0) + \Delta$ crosses the calculated values of $B_Y(k=0)$. This is indicated by the dotted lines in the figure. In the case of the Nijmegen interaction we obtain $\omega = -74.3 \text{ MeV}$ ($B_\Lambda(0) = -24.3 \text{ MeV}$) for the Λ and $\omega = 15.8 \text{ MeV}$ ($B_\Sigma(0) = -11.7 \text{ MeV}$) for the Σ , whereas, in the case of the Jülich interaction, $\omega = -80.2 \text{ MeV}$ for the Λ ($B_\Lambda(0) = -30.2 \text{ MeV}$) and $\omega = -36.0 \text{ MeV}$ ($B_\Sigma(0) = -63.5 \text{ MeV}$) for the Σ .

Several features emerge from Fig. 2. First, the Σ hyperon is unrealistically overbound in nuclear matter by the Jülich interaction. It is therefore necessary to readjust the parameters of this interaction if one wants to use it in shell model calculations of Σ hypernuclei. Secondly, we observe that the energy dependence of $U_Y(k=0)$ is slightly stronger in the case of the Nijmegen interaction, especially for the Σ hyperon which is more sensitive to the $\Sigma N - \Lambda N$

coupling because the starting energy is closer to the energies of the intermediate ΛN states (which propagate with the kinetic energy spectrum). Finally, we observe that the Λ binding energy varies at most by 10 MeV in a starting energy range of 80 MeV, while the variation of the Σ binding amounts to twice as much. As we will see below, this has consequences in the results for finite hypernuclei.

In Tables I and II we show the binding energy of the Λ and Σ^0 , respectively, in ${}^{17}_Y\text{O}$. The columns denoted by HF correspond to our lowest order calculation (see Eq. (15)) which uses, as effective interaction, the nuclear matter G -matrix calculated in the YN center of mass frame at fixed energy (shown in the first column) and density ($k_F = 1.36 \text{ fm}^{-1}$). Columns labelled $(HF + 2p1h)$ include the $2p1h$ corrections (see Eqs. (17) and (18)) to bring the nuclear matter G -matrix to the finite nucleus one, with the proper energy and density dependence. We see that the lowest order results depend quite strongly on the starting energy used, especially in the case of the Σ hyperon as would be expected from the nuclear matter results shown in Fig. 2. However, it is worth noticing how, no matter what starting energy is used in solving the nuclear matter G -matrix, the corrected calculation ($HF + 2p1h$) ends up giving practically the same result for the hyperon binding energy. Particularly stable are the results for the Λ hyperon. This weaker energy dependence, seen already in the nuclear matter results of Fig. 2, is due to the fact that the energies involved in the calculation lie further away from the intermediate YN states, which propagate with kinetic energy, and therefore the strong $\Lambda N - \Sigma N$ coupling is less pronounced.

In Tables III and IV we show the binding energy of the Λ and Σ^0 , respectively, in ${}^{17}_Y\text{O}$ using nuclear matter G -matrices calculated at several values of the Fermi momentum and a fixed value of the starting energy ($\omega = -50$ for the Λ and $\omega = 0$ for the Σ). The lowest order calculation for the hyperon single-particle energy, shown in the second column, depends quite strongly on the value of k_F . However, one finds again that, when the $2p1h$ correction is included to incorporate the proper intermediate propagator of the finite nucleus, the results nicely converge to practically the same value, no matter what was the density used in the solution of the nuclear matter G -matrix.

These results are interesting because they confirm that the finite nucleus G_{FN} -matrix is already well approximated by the second order term in the expansion in terms of the nuclear matter G -matrix, see the second and third terms in Eq. (8). The correction, whose size depends on the starting energy or Fermi momentum used in the solution of the nuclear matter G -matrix, already leads to practically the same value for the hyperon single-particle energy. Higher order terms could only help in bringing the results closer than what they already are. Moreover, our results also show that in some cases the correction is quite appreciable, not only for the Σ^0 binding energies shown in Tables II and IV, but also for the Λ energies in the case of the Nijmegen interaction. Therefore, if the correction is taken only approximately through an averaged nuclear matter G -matrix [37–40] it may not lead to the proper effective interaction in the finite nucleus one is studying. These words of caution are particularly relevant in the case of the Σ hyperon where the corrections are very large.

We note that the Λ single-particle energy obtained in the case of the Nijmegen soft core interaction is in excellent agreement with that obtained by Halderson (see column 3 in Fig. 7 of Ref. [41]), where the G -matrix was calculated directly in the finite nucleus for various Nijmegen interactions. Our method must be viewed as an alternative way of building up a finite nucleus effective interaction. It was already shown there that the Pauli corrections, which are a source of nucleus dependence, were very large for the Nijmegen soft core potential. This again supports our believe that calculations based on nuclear matter G -matrices at an average density will carry uncertainties tied to the chosen value of the Fermi momentum. In particular, the whole purpose of using these microscopic calculations to constrain the YN force cannot be achieved if a different value of k_F is used for each YN interaction when studying the same hypernucleus [39].

In the studies of single-particle binding energies below, we will refrain from a study of the Σ binding energy since the results for $^{17}_{\Sigma}\text{O}$ give single-particle binding energies which are much too attractive. Several analysis of Σ^- atomic data [50,51] suggest a Σ well depth similar to that of the Λ [52,53] and more recent analysis [54,55] did not discard Σ -nucleus potentials showing an inner repulsion. Moreover, Σ hypernuclear spectra from (K^-, π^-) reactions

suggest a relatively shallow Σ -nucleus potential [4]. Therefore, although the amount of data is limited, there is no experimental evidence for such strongly bound Σ hyperons. This clearly points to a weakness in the present YN interactions, hinting possibly at a too strong $\Sigma N - \Lambda N$ coupling in the interactions.

B. Λ Single-particle states

Once the method is well established and tested for the specific case of ${}_{\Lambda}^{17}\text{O}$, it is the right moment to study the systematics of the Λ binding energy through the periodic table. To this end, values of the Λ single-particle binding energies obtained in what has been called HF and $HF + 2p1h$ approximations are reported in Table V together with the available experimental data. These binding energies have been calculated using the energy-independent version with parameter set B of the Jülich potential [47]. The results for the Nijmegen soft core potential [46] have not been considered in this section because the corresponding prediction for the Λ binding energy in nuclear matter is -23.4 MeV, about 7 MeV weaker than the prediction of the Jülich model (-30.2 MeV) which agrees well with the extrapolated experimental values of the single-particle Λ binding energies with increasing mass number.

The agreement with the experimental data is rather good. For convenience in the technicalities of the algorithm we have always considered hypernuclei with a number of nucleons closing a subshell plus a Λ . Unfortunately, experimental data for those nuclei do not always exist and, as indicated in the Table V, we have taken the closest representative nucleus for which the experimental information is available. Nevertheless, the differences between the calculated and the experimental values should not be associated to this fact but to the approximations used in the calculation or to the potential itself.

For the density and starting energy used to calculate the Λ -nucleon G -matrix in nuclear matter, which has been used as effective interaction in our finite nucleus calculation, it turns out that the $2p1h$ correction is always attractive. As discussed in the previous section, if we had used other starting values for the density or the starting energy we would have ended

up with different $2p1h$ corrections but with the same value for $HF + 2p1h$.

In agreement with the experimental information, the difference between the $p_{3/2}$ and $p_{1/2}$ Λ single-particle binding energies associated to these partial waves is very small. Note that the $p_{1/2}$ energy is lower than the $p_{3/2}$. This is a characteristic of the Jülich interaction which yields too much attraction in the 3S_1 partial wave, as noted already in [39,40] where the 0^+ and 1^+ states of ${}^4_\Lambda\text{He}$ were calculated and showed to appear in reverse order from the experimental values.

The calculated Λ single-particle energies for ${}^{209}_\Lambda\text{Pb}$ appear clearly overbound with respect to the experimental data. This is due to the fact that the distortion of the plane wave associated with the nucleon in the intermediate state of the $2p1h$ diagram of Fig. 1(b), necessary to ensure its orthogonalization to the nucleon hole states, has been taken only approximately. The orthogonalization procedure is described in Ref. [44] and has been optimized for the case of ${}^{17}_\Lambda\text{O}$. Actually, this feature is already sizable for ${}^{91}_\Lambda\text{Zr}$ and in the case of ${}^{209}_\Lambda\text{Pb}$ leads to a result which is more bound than a Λ in nuclear matter.

Traditionally, the systematics of Λ single-particle binding energies has been studied by using a phenomenological Woods-Saxon potential

$$V_{WS}(r) = \frac{V_0}{1 + \exp [(r - R)/a]}, \quad (22)$$

with a fixed diffusivity a and depth V_0 , and a radius $R = r_0 A^{1/3}$. A good parameterization of the experimental data is obtained with $V_0 = -30.7$ MeV, $r_0 = 1.1$ fm and $a = 0.6$ fm [25]. A more refined analysis of the same authors allows for a smooth dependence of r_0 in A and a slightly shallower potential ($V_0 = -28$ MeV) with a larger radius, $r_0(A) = (1.128 + 0.439A^{-2/3})$ fm, provides a better agreement with the experimental Λ binding energies. We have performed a similar analysis for the calculated Λ binding energies. In principle, the calculated self-energy is non-local both in k -space and in r -space. However, in a previous work [43] we have shown that one can generate a local representation of the self-energy by performing an appropriate average of the non-local self-energy $\Sigma_\alpha(r, r')$, where α indicates the quantum numbers of the single-particle state, over the coordinate r' .

This local representation might, in first approximation, be characterized by the shape of a Woods-Saxon potential. Instead of doing this average, a possible strategy is to assume a Woods-Saxon shape, fix the depth and the diffusivity independent of the mass number and determine the radius R by requiring the Woods-Saxon potential to reproduce the same eigenvalue than the microscopic non-local energy dependent self-energy. A reasonable value for the depth V_0 is the Λ binding energy in nuclear matter, which is taken to be -30.2 MeV, and for the diffusivity $a = 0.6$ fm. The resulting values of R when we apply this procedure to the s deepest state of ${}^{13}_{\Lambda}\text{C}$, ${}^{17}_{\Lambda}\text{O}$ and ${}^{41}_{\Lambda}\text{Ca}$ are 2.25 fm, 2.53 fm and 3.82 fm respectively. Fitting these three values with a functional form similar to the one used in Ref. [25] for the analysis of the experimental data one obtains $r_0(A) = (1.229 - 1.390A^{-2/3})$ fm. In order to visualize the quality of these fits, we show in Fig. 3 the binding energies for the s and p waves of ${}^{12}_{\Lambda}\text{C}$, ${}^{17}_{\Lambda}\text{O}$, ${}^{41}_{\Lambda}\text{Ca}$ and ${}^{91}_{\Lambda}\text{Zr}$ calculated with our non-local self-energies (triangles) together with the values obtained with a Woods-Saxon potential with the parameters just defined above (solid lines). As the spin-orbit splitting is so small we have reported the average value of the $p_{3/2}$ and $p_{1/2}$ energies obtained from the non-local self-energies and have not considered any spin-orbit term in the adjusted Woods-Saxon potential. The results of ${}^{209}_{\Lambda}\text{Pb}$ have not been included in the plot because, as mentioned before, the s wave binding energy was larger than the binding energy in nuclear matter which we have taken as the depth of the Woods-Saxon potential. The calculated binding energies are well reproduced by the Woods-Saxon shape and, as expected, both partial waves extrapolate to the binding energy for nuclear matter.

Of course the binding energies are not enough to characterize the single-particle states since potentials giving rise to the same binding energies can generate substantial differences in the corresponding wave functions. Therefore, in order to analyze the microscopically calculated self-energy we should also study the single-particle wave functions.

To have a measure of the goodness of the wave functions generated by the Woods-Saxon potential, we calculate their overlap with the wave functions obtained by solving the Schrödinger equation using the self-energy. The overlaps for ${}^{13}_{\Lambda}\text{C}$, ${}^{17}_{\Lambda}\text{O}$, ${}^{41}_{\Lambda}\text{Ca}$ and ${}^{91}_{\Lambda}\text{Zr}$ are

0.9917, 0.9869, 0.9924 and 0.9853 respectively, which are not close enough to 1 to guarantee the equality of the wave functions. This is visualized in Fig. 4, where the wave function for the s wave in ${}^{17}_{\Lambda}\text{O}$ obtained with the Woods-Saxon potential (dashed-line) is compared with the one obtained directly from the self-energy (solid line).

Another possibility would be to keep the diffusivity fixed and adjust the radius R and the depth V_0 to reproduce the eigenvalue and to maximize the overlap with the eigenfunction provided by the self-energy. The values of V_0 by applying this procedure to the s wave of the three lighter nuclei considered above are respectively -23.11 , -23.56 and -27.84 MeV whereas the values of the radius R are 2.92, 3.32 and 4.39 fm. With these values of V_0 and R the overlaps are 0.9999 for the three nuclei considered. The eigenfunction obtained by this procedure for the ${}^{17}_{\Lambda}\text{O}$ is also drawn in Fig. 4 (dot-dashed line) and shows a large overlap with the self-energy eigenfunction (solid-line).

In conclusion, the single-particle energies of closed-shell nuclei with one Λ are well reproduced by using both the microscopic self-energy or the simpler parametrization of Woods-Saxon type in the Schrödinger equation. However, the wave functions provided by the microscopic self-energy differ from the ones originated by a Woods-Saxon with a fixed depth and diffusivity and a A -dependent radius. It is important to note that the mean square radius of the self-energy eigenfunction is larger than that from the corresponding Woods-Saxon wave function. This can have important consequences in the study the mesonic decay of these Λ hypernuclei. Indeed, it has been observed that the mesonic decay rates of light hypernuclei, such as ${}^4_{\Lambda}\text{H}$, ${}^4_{\Lambda}\text{He}$ and ${}^5_{\Lambda}\text{He}$, could be better reproduced if the Λ wave function was pushed out to the surface by the effect of a repulsive hyperon-nucleus potential at short distances. This would favour the mesonic decay of these hypernuclei because the Λ would be exploring smaller nuclear density regions and the Pauli blocking effects, which prevent the mesonic decay from occurring, would be less pronounced. The mesonic decay rates of light hypernuclei have been calculated using repulsive Λ -nucleus potentials at short distances that have been obtained either phenomenologically [16], from a quark based bare YN interaction [15] or from a microscopic YNG effective interaction folded with an extremely compact ${}^4\text{He}$ density

[14]. At present, no calculation exists that combines the use of an YN effective interaction with an appropriate density treatment of the host nucleus. Our method provides such ingredients and has been shown to produce Λ wave functions that are pushed out to the surface. This is a consequence of the non-localities of the self-energy and might not be related to a repulsive character of the Λ -nucleus potential at short distances. The implications of our results on the mesonic decay of Λ hypernuclei will be explored in a future work.

IV. CONCLUSIONS

We have analyzed a method to obtain the effective hyperon-nucleon interaction in finite nuclei based on an expansion over a G -matrix calculated in nuclear matter at fixed density and starting energy. The purpose of this study is to set up a reliable frame for hypernuclear structure calculations with the aim of obtaining information about the hyperon-nucleon interaction, complementary to that provided by hyperon-nucleon scattering experiments.

We have shown, by explicit calculation of the Λ and Σ single-particle energies in ${}^{17}_Y\text{O}$, that truncating the expansion over the nuclear matter G -matrix at second order gives results that are very stable against variations of the density and starting energy used in the G -matrix. Moreover, both first and second order terms depend quite strongly on those parameters. This is an indication that the density dependent effects considered when treating explicitly the finite size of the nucleus are very important and, therefore, they might not be well approximated by energy independent and local effective interactions which start from a parametrized nuclear matter G -matrices evaluated at an average density. We note that the use of local and density averaged effective interactions can be extremely useful in detecting similarities and differences among the various hyperon-nucleon potentials. However, if the aim is to fine-tune the bare YN interactions to reproduce the spectroscopic data of hypernuclei, an appropriate effective interaction for the hypernucleus under study, as the one provided by our method, is in order. In particular, the two interactions employed in the present work give rise to very attractive Σ binding energies, while the Σ^- atomic data and

(K^-, π^-) spectra seem to indicate Σ -nucleus potential depths similar to that of the Λ or even shallower.

Although the method can be viewed as an alternative way of building up a finite nucleus effective interaction, it provides also the complete energy dependence of the hyperon self-energy. This allows in turn for a study of not only the bound states, as done here, but also the scattering states. This is especially of interest in the analysis of hypernuclear production reactions which yield a large amount of quasifree hyperons.

We have obtained local Woods-Saxon Λ -nucleus potentials that reproduce the Λ single-particle energies of several hypernuclei. However, the wave functions obtained from our non-local self-energy are far more extended and can be simulated only when we allow the Woods-Saxon potential to have an A -dependent depth and a relatively larger radius. This can have important implications on the weak mesonic decay of Λ hypernuclei, which will be explored in a future work.

V. ACKNOWLEDGEMENTS

This work is partially supported by the DGICYT contract No. PB95-1249 (Spain) and by the Generalitat de Catalunya grant No. GRQ94-1022. One of the authors (I.V.) wishes to acknowledge support from a doctoral fellowship of the Ministerio de Educación y Cultura (Spain).

REFERENCES

- [1] A. Gal, *Adv. Nucl. Sci.* 8 (1977) 1.
- [2] B. Povh, *Ann. Rev. Nucl. Part. Sci.* 28 (1978) 1.
- [3] H. Bandō, K. Ikeda, T. Motoba, Y. Yamada and T. Yamamoto, *Prog. Theor. Phys. Suppl.* 81 (1985).
- [4] C.B. Dover, D.J. Millener and A. Gal, *Phys. Rep.* 184 (1989) 1.
- [5] E. Oset, P. Fernández de Córdoba, L.L. Salcedo and R. Brockmann, *Phys. Reports* 188 (1990) 79.
- [6] J. Cohen, *Prog. Part. Nucl. Phys.* 25 (1990) 139.
- [7] H. Bandō, T. Motoba and J. Žofka, *Int. J. Mod. Phys. A5* (1990) 4021.
- [8] B.F. Gibson and E.V. Hungerford, *Phys. Reports* 257 (1995) 349.
- [9] Y. Akaishi and T. Yamazaki, *Prog. Part. Nucl. Phys.* 39 (1997) 565.
- [10] E. Oset and A. Ramos, *Prog. Part. Nucl. Phys.* 41 (1998), in press.
- [11] W. Brückner et al., *Phys. Lett.* 79B (1978) 157.
- [12] P.H. Pile et al, *Phys. Rev. Lett.* 66 (1991) 2585.
- [13] T. Hasegawa et al, *Phys. Rev.* C53 (1996) 1210.
- [14] T. Motoba, H. Bandō, T. Fukuda and J. Žofka, *Nucl. Phys.* A534 (1991) 597.
- [15] U. Straub, J. Nieves, A. Faessler and E. Oset, *Nucl. Phys.* A556 (1993) 531.
- [16] I. Kumagai-Fuse, S. Okabe and Y. Akaishi, *Phys. Lett.* B345 (1995) 386.
- [17] J.J. Szymanski et al., *Phys. Rev.* C43 (1991) 849.
- [18] T. Harada, S. Shinmura Y. Akaishi and H. Tanaka, *Nucl. Phys.* A507 (1990) 715.

- [19] T. Nagae et al, Phys. Rev. Lett. 80 (1998) 1605.
- [20] R.S. Hayano et al, Nuovo Cimento 102A (1989) 437; Phys. Lett. B231 (1989) 355.
- [21] A. Bouyssy, J. Hüfner, Phys. Lett. 64B (1976) 276; A. Bouyssy, Phys. Lett. 84B (1979) 41.
- [22] C. Dover, L. Ludeking and G.E. Walker, Phys. Rev. C22 (1980) 2073.
- [23] T. Motoba, H. Bandō, R. Wünsch and J. Žofka, Phys. Rev. C38 (1988) 1322.
- [24] Y. Yamamoto, H. Bandō and J. Žofka, Prog. Theor. Phys. 80 (1988) 757.
- [25] D.J. Millener, C.B. Dover and A. Gal, Phys. Rev. C38 (1988) 2700.
- [26] F. Fernández, T. López-Arias and C. Prieto, Z. Phys. A334 (1989) 349.
- [27] D.E. Lansky and Y. Yamamoto, Phys. Rev. C55 (1997) 2330.
- [28] R. Brockmann and W. Weise, Nucl. Phys. A355 (1981) 365.
- [29] M. Chiapparini, A.O. Gattone and B.K. Jennings, Nucl. Phys. A529 (1991) 589.
- [30] J. Mareš and J. Žofka, Z. Phys. A33 (1989) 209.
- [31] J. Mareš and B.K. Jennings, Phys. Rev. C49 (1994) 2472.
- [32] R.J. Lombard, S. Marcos and J. Mareš, Phys. Rev. C51 (1995) 1784.
- [33] N.K. Glendenning, D. Von-Eiff, M. Haft, H. Lenske and M.K. Weigel, Phys. Rev. C48 (1993) 889.
- [34] F. Ineichen, D. Von-Eiff and M.K. Weigel, J. Phys. G22 (1996) 1421.
- [35] Y. Sugahara and H. Toki, Prog. Theor. Phys. 92 (1994) 803.
- [36] Z. Ma, J. Speth, S. Krewald, B. Chen and A. Reuber, Nucl. Phys. A608 (1996) 305.
- [37] Y. Yamamoto and H. Bandō, Prog. Theor. Phys. Suppl. 81 (1985) 9; K. Tsushima,

- K. Saito and A. W. Thomas, Phys. Lett. B411 (1997) 9; K. Tsushima, K. Saito, J. Haidenbauer and A. W. Thomas, Nucl. Phys. A630 (1998) 691.
- [38] Y. Yamamoto and H. Bandō, Prog. Theor. Phys. 83 (1990) 254.
- [39] Y. Yamamoto, A. Reuber, H. Himeno, S. Nagata and T. Motoba, Czec. Jour. Phys. 42 (1992) 1249.
- [40] Y. Yamamoto, T. Motoba, H. Himeno, K. Ikeda and S. Nagata, Prog. Theor. Phys. Suppl. 117 (1994) 361.
- [41] D. Halderson, Phys. Rev. C48 (1993) 581.
- [42] J. Hao, T.T.S. Kuo, A. Reuber, K. Holinde, J. Speth and D.J. Millener, Phys. Rev. Lett. 71 (1993) 1498.
- [43] M. Hjorth-Jensen, A. Polls, A. Ramos and H. Mütter, Nucl. Phys. A605 (1996) 458.
- [44] M. Borromeo, D. Bonatsos, H. Mütter and A. Polls, Nucl. Phys. A539 (1992) 189.
- [45] M. Hjorth-Jensen, H. Mütter and A. Polls, Phys. Rev. C50 (1994) 551.
- [46] P.M.M. Maessen, T.A. Rijken, and J.J. de Swart, Phys. Rev. C40, 2226 (1989).
- [47] B. Holzenkamp, K. Holinde, and J. Speth, Nucl. Phys. A500, 485 (1989).
- [48] C.L. Kung, T.T.S. Kuo and K.F. Ratcliff, Phys. Rev. C19 (1979) 1063
- [49] C.W. Wong and D.M. Clement, Nucl. Phys. A183 (1972) 210
- [50] G. Backenstoss, T. Bunacin, J. Egger, H. Koch, A. Schwitter and L. Tauscher, Z. Phys. A273 (1975) 137
- [51] C. J. Batty et al, Phys. Lett. 74B (1978) 27
- [52] C. J. Batty, Phys. Lett. 87B (1979) 324
- [53] C. J. Batty, Nucl. Phys. A372 (1981) 433

- [54] C. J. Batty, E. Friedman and A. Gal, Phys. Lett. 335 (1994) 273; Prog. Theor. Phys. Suppl. 117 (1994) 227
- [55] J. Mareš, E. Friedman, A. Gal and B. K. Jennings, Nucl. Phys. A594 (1995) 311

TABLES

TABLE I. Dependence of the Λ single-particle energy in ${}^{17}_{\Lambda}\text{O}$ on the starting energy of the nuclear matter G -matrix. Our notation is $\omega = \langle B_N \rangle + B_{\Lambda}(k = 0)$, with $\langle B_N \rangle = -50$ MeV.

$k_F = 1.36 \text{ fm}^{-1}$	Nijmegen		Jülich	
ω (MeV)	HF (MeV)	$HF + 2p1h$ (MeV)	HF (MeV)	$HF + 2p1h$ (MeV)
-100	-3.83	-7.43	-9.25	-11.85
-80	-4.76	-7.39	-10.15	-11.83
-50	-5.59	-7.36	-11.73	-11.84

TABLE II. Dependence of the Σ^0 single-particle energy in ${}^{17}_{\Sigma^0}\text{O}$ on the starting energy of the nuclear matter G -matrix. Our notation is $\omega = \langle B_N \rangle + B_{\Sigma}(k = 0) + \Delta$, with $\langle B_N \rangle = -50$ MeV and $\Delta = M_{\Sigma} - M_{\Lambda}$.

$k_F = 1.36 \text{ fm}^{-1}$	Nijmegen		Jülich	
ω (MeV)	HF (MeV)	$HF + 2p1h$ (MeV)	HF (MeV)	$HF + 2p1h$ (MeV)
0	-0.16	-22.79	-36.70	-50.70
20	-2.01	-23.35	-40.38	-50.94
50	-10.65	-24.62	-51.34	-50.38

TABLE III. Dependence of the Λ single-particle energy in ${}^{17}_{\Lambda}\text{O}$ on the Fermi momentum of the nuclear matter G -matrix. Our notation is $\omega = \langle B_N \rangle + B_{\Lambda}(k = 0)$, with $\langle B_N \rangle = -50$ MeV.

$\omega = -50$ MeV	Nijmegen		Jülich	
k_F (fm $^{-1}$)	HF (MeV)	$HF + 2p1h$ (MeV)	HF (MeV)	$HF + 2p1h$ (MeV)
1.00	-9.33	-7.30	-13.71	-11.74
1.25	-7.66	-7.34	-12.56	-11.83
1.36	-5.59	-7.36	-11.73	-11.84

TABLE IV. Dependence of the Σ^0 single-particle energy in ${}^{17}_{\Sigma^0}\text{O}$ on the Fermi momentum of the nuclear matter G -matrix. Our notation is $\omega = \langle B_N \rangle + B_{\Sigma}(k = 0) + \Delta$, with $\langle B_N \rangle = -50$ MeV and $\Delta = M_{\Sigma} - M_{\Lambda}$.

$\omega = 0$ MeV	Nijmegen		Jülich	
k_F (fm $^{-1}$)	HF (MeV)	$HF + 2p1h$ (MeV)	HF (MeV)	$HF + 2p1h$ (MeV)
1.00	-2.64	-25.03	-43.94	-51.74
1.25	-0.82	-23.37	-39.41	-51.16
1.36	-0.16	-22.79	-36.70	-50.70

TABLE V. Λ binding energies in the $1s_{1/2}$, $1p_{3/2}$ and $1p_{1/2}$ single-particle orbits for different nuclei. The available experimental data, indicating the hypernucleus for which they have been measured, are taken from the compilation of [7] supplemented by new measures reported in [12] and [13]. All the results have been derived from the Jülich B interaction.

Hypernuclei	Orbit	HF	$HF + 2p1h$	Exp
${}_{\Lambda}^{13}\text{C}$	$1s_{1/2}$	-7.93	-9.48	$({}_{\Lambda}^{13}\text{C})$ -11.69
${}_{\Lambda}^{17}\text{O}$	$1s_{1/2}$	-10.15	-11.83	$({}_{\Lambda}^{16}\text{O})$ -12.5
	$1p_{3/2}$		-0.87	-2.5 (1p)
	$1p_{1/2}$	-0.08	-1.06	
${}_{\Lambda}^{41}\text{Ca}$	$1s_{1/2}$	-16.85	-19.60	$({}_{\Lambda}^{40}\text{Ca})$ -20.
	$1p_{3/2}$	-6.70	-9.64	-12. (1p)
	$1p_{1/2}$	-6.92	-9.92	
${}_{\Lambda}^{91}\text{Zr}$	$1s_{1/2}$	-22.24	-25.80	$({}_{\Lambda}^{89}\text{Zr})$ -23.
	$1p_{3/2}$	-14.74	-18.19	-16. (1p)
	$1p_{1/2}$	-14.86	-18.30	
${}_{\Lambda}^{209}\text{Pb}$	$1s_{1/2}$	-26.28	-31.36	$({}_{\Lambda}^{208}\text{Pb})$ -27.
	$1p_{3/2}$	-21.22	-27.13	-22. (1p)
	$1p_{1/2}$	-21.30	-27.18	

FIGURES

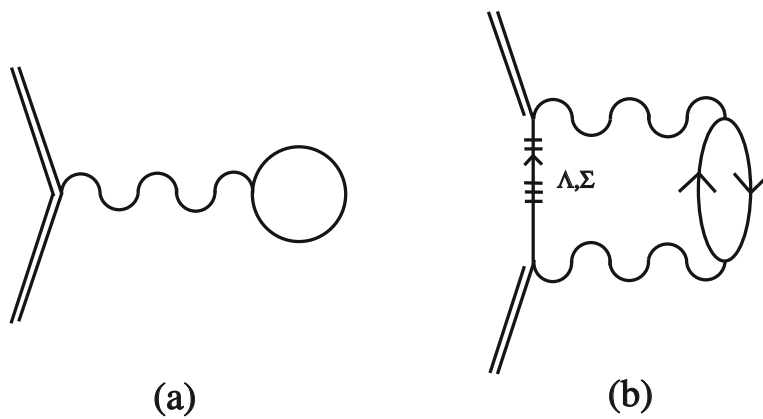


FIG. 1. Diagrams through second order in the interaction $YN G$ (wavy line) included in the evaluation of the hyperon self-energy. Diagram (a) is the first order term, while (b) is the second order $2p1h$ correction.

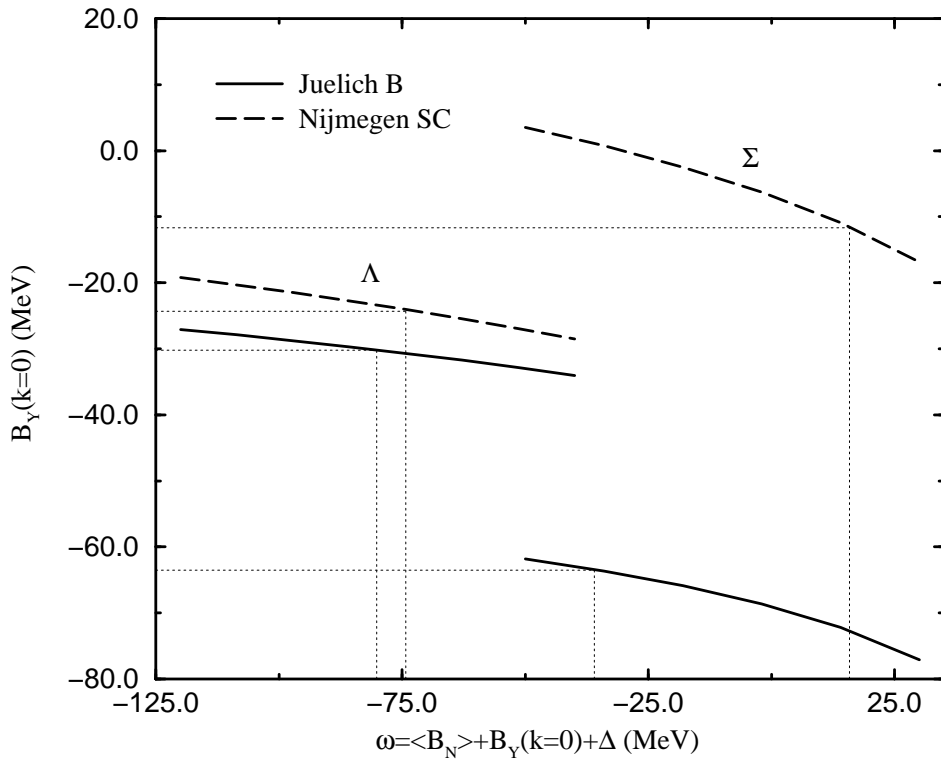


FIG. 2. Dependence of the hyperon binding energy $B_Y(k = 0)$ in nuclear matter on the starting energy ω . The curves on the left are for the Λ , whereas the ones on the right are for the Σ . Long-dashed (full) lines correspond to Nijmegen soft core (Jülich B) interaction. The dotted lines show the position of the self-consistent solution for $B_Y(k = 0)$.

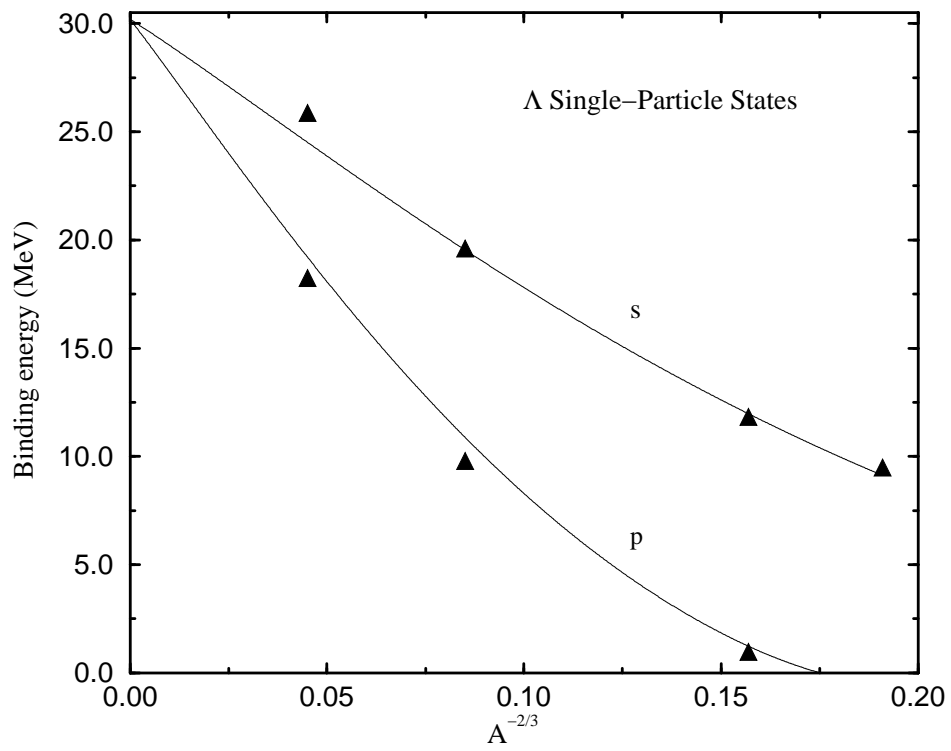


FIG. 3. Calculated Λ binding energies in $1s$ and $1p$ single-particle orbits for different nuclei. The curves correspond to the solutions obtained for a Woods-Saxon potential whose parameters are defined in the text.

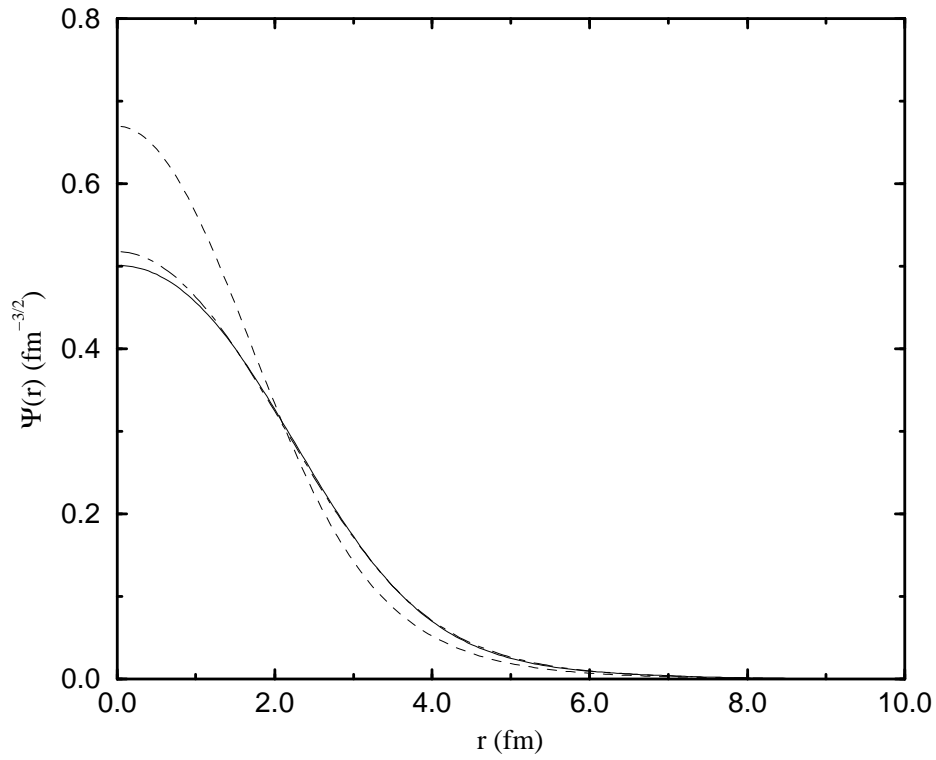


FIG. 4. The wave function in r -space for the $1s_{1/2}$ Λ in ${}^{17}_{\Lambda}\text{O}$ obtained from the Λ self-energy (solid line) is compared with the ones obtained using a Woods-Saxon potential of fixed (A -independent) depth (dashed line) or with both radius and depth adjusted (dot-dashed line) to maximize the overlap with the wave function provided by the self-energy.